ELSEVIER

Journal of Nuclear Materials 303 (2002) 105–114

journal of nuclear materials

www.elsevier.com/locate/jnucmat

A model for analyzing corrosion data from pulsed proton beam irradiation experiments

R.S. Lillard *, M.A. Paciotti [1]

Materials Corrosion and Environmental Effects Lab, Materials Science and Technology Division, MST-6, Los Alamos National Laboratory, P.O. Box 1663, MS G755, Los Alamos, NM 87545, USA

Received 18 December 2001; accepted 1 April 2002

Abstract

A model for analyzing corrosion data from pulsed proton beam irradiation experiments was developed from time-averaged corrosion rate measurements taken as a function of beam duty cycle and peak (instantaneous) beam current. The model assumes that there are two separate processes that control corrosion kinetics at the solution–metal interface: one during proton pulses and one between pulses. The model was evaluated using two techniques: a simulation program with integrated circuit emphasis (an integrated circuit analysis routine) and a numerical method. The model found that the corrosion rate between proton pulses was two orders of magnitude lower than the corrosion rate during a proton pulse. In addition, the model predicts that the corrosion rate during a pulse of protons correlates with peak current and that the time-average corrosion rate is weighted more heavily for duty cycle (repetition rate and gate length) than peak current. These findings explain apparent anomalies in time-averaged corrosion data; it was observed that for a fixed average beam current that the time-averaged corrosion rate for a 16 mA peak current was lower than the time-averaged corrosion rate at a peak current of 1.6 mA. This apparent anomaly is explained in the model by the higher duty cycle for the 1.6 mA case. © 2002 Published by Elsevier Science B.V.

1. Introduction

Spallation neutron source target/blanket cooling loops present a unique combination of parameters that may influence the corrosion rates of metals, including high energy protons, high and low energy neutrons, gamma radiation, and water radiolysis products. In previous publications, Lillard and Butt have described a novel method for measuring the corrosion rate of materials in spallation neutron sources [1–3]. In these experiments, the real-time corrosion rate of alloy 718 was measured with electrochemical impedance spectroscopy (EIS) during irradiation in an 800 MeV proton beam at the Los Alamos Neutron Science Center (LANSCE). Because the proton beam spot size was smaller than the sample, two methods were employed for determining corrosion rate from polarization resistance. The first method assumed that the distribution of corrosion was uniform across the entire probe surface. The second method used proton flux as a criterion for determining the area of highest damage. The foundation for the flux model was based on thickness measurements from tungsten rods irradiated in a separate cooling water loop at LANSCE. In that work, Sommer et al., found that the post irradiation thickness profiles of W rods, irradiated at a beam current of 1.0 mA for approximately two months, were Gaussian and corresponded to the Gaussian profile of the beam [4]. However, later work demonstrated that proton flux could not satisfactorily explain observed distributions in corrosion rate for other materials [5].

In this paper we investigate the influence of the pulsed nature of the proton beam on experimental methods for

* Corresponding author. Tel.: +1-505 667 6325; fax: +1-505 667 8021.

E-mail address: lillard@lanl.gov (R.S. Lillard).

[1] Advanced Accelerator Applications Group, Los Alamos Neutron Science Center.

0022-3115/02/$ - see front matter © 2002 Published by Elsevier Science B.V.
PII: S0022-3115(02)00848-6

measuring corrosion rate. The beam at LANSCE delivers protons to the target in a series of pulses characterized by a peak current, macropulse length, and repetition rate. This combination of parameters is referred to as the duty cycle. The pulse length being on the order of 200–600 μs while the repetition rate on the order of 10–100 Hz. Therefore, given the pulsed nature of the beam, one might assume that the electrochemical kinetics at the surface respond in a similar manner as the beam is delivered to the surface; brief periods of very high corrosion rates spaced between periods of low (or decreasing) corrosion rates. In contrast to these relatively short duty cycle times are the acquisition times required to make corrosion rate measurements. Whether EIS, Tafel extrapolation, or linear polarization resistance is used, the experimental techniques available assume that corrosion rate is constant over a period of minutes or even hours. The purpose of this work was to develop a duty cycle based model to understand the electrochemical response of a target during pulsed proton irradiation and, more importantly, determine whether or not traditional time-averaged methods for measuring corrosion rate accurately measure this process.

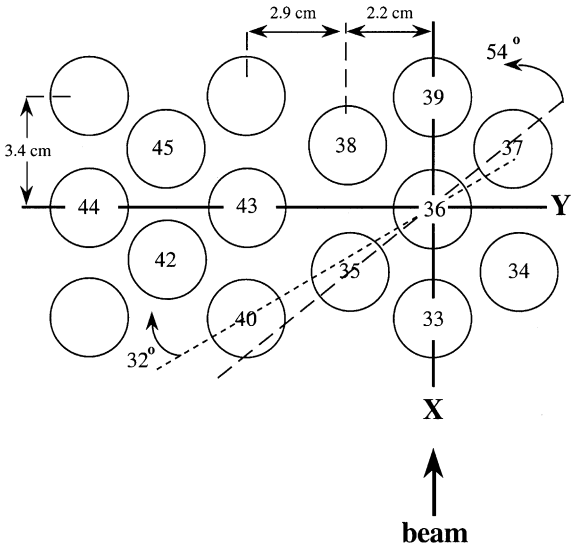

Fig. 1. A perspective of the tube array from the front, top-down. The path of the proton beam was parallel to the X axis at $Y = 0$. Here we have defined the center of tube #36 as (0,0). Each numbered tube contained a corrosion probe. Alloy 718: 33, 39, and 45; SS 316L: 35, 36, 38, and 40; Al6061: 42, 43, and 44; Ni super alloys: 34 and 37.

2. Experimental

2.1. The in-beam corrosion loop

All experiments were conducted at the A6 Target Station of LANSCE. A detailed description as well as diagrams of the beam line at A6, the corrosion water loop, and probe design have been presented elsewhere [3]. Briefly, the corrosion water loop consisted of a water pumping system that supplied a manifold with circulating water. This manifold held the corrosion samples in-beam and provided water cooling of the samples. With the exception of the individual corrosion samples, the system was fabricated entirely of type 304 stainless steel (SS). To measure real-time in-beam corrosion rates, a special probe was designed to isolate electrically the corrosion samples from the SS plumbing system [1–3]. The water manifold that held these probes consisted of 15 flow tubes arranged in close-packed arrays (Fig. 1). Each tube contained either an in-beam corrosion probe or a flow restrictor (unnumbered tubes in Fig. 1). With respect to water flow, tubes 33–39 were in parallel with one another and in series with tubes 40–45 (which were also in parallel with one another). The manifold was welded to the bottom of a 3.4 m supporting insert that not only supported the weight of the manifold but also provided the necessary conduits for electrical and water connections. Thermocouples attached to the front of the manifold verified the position, size, and shape of the proton beam.

2.2. Sample preparation and water quality

The corrosion rates of two materials will be discussed in this paper: stainless steel 316L (SS 316L, UNS31603 Cr-18 wt%, Ni-14, Mn-2, Mo-3, Si-1, and Fe-bal.) and alloy 718 (UNS N07718, precipitation hardened, Cr-18 wt%, Fe-19, Nb-5, Mo-3, Ti-1, and Ni-53 min). Results from aluminum and nickel superalloys are presented elsewhere [5]. To provide a fresh metal surface for electrochemical characterization, all samples were ground with metallographic SiC papers to 400 p (European grade). After grinding, the samples were degreased in an ultrasonic bath of acetone. Degreasing was followed by successive sonications in ethanol and deionized water. Prior to placing the probes in the water system, the interior of the water system, which included all piping, tanks, and pumps, was cleaned as previously described [3]. The water resistivity varied between 1×10^6 Ω cm (initial) and 8×10^4 Ω cm (after several weeks of operation). Nominally, the system operated at an inlet water temperature between 18 °C (beam off) and 24 °C (beam at 0.340 mA), a pressure of 1.02 MPa, and a total flow rate of 0.91 L/s. This resulted in a flow rate of 0.13 L/s for the in-beam probes (tubes 33–39) and 0.11 L/s for the near-beam probes (tubes 40–45), and a water velocity of 1.21 m/s. The resulting Reynolds numbers for the in-beam and near-beam tubes were 6214 and 5434 respectively (calculated at 25 °C). In an attempt to mitigate the formation of water radiolysis

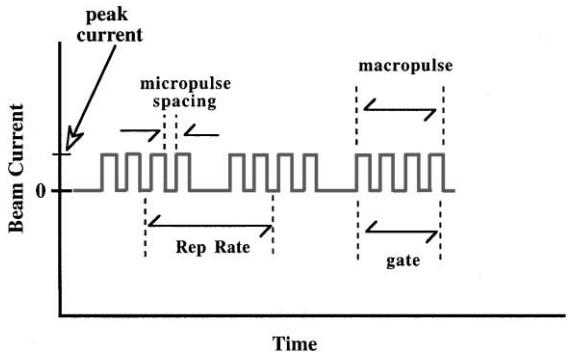

Fig. 2. A diagram depicting the proton beam profile (i.e. the duty cycle) at the LANSCE A6 Target Station.

products such as H_2O_2 [6–9], the system was operated with a dissolved hydrogen concentration of ≈0.40 mol/m^3. This was accomplished by continuously bubbling 6% H_2 – 94% Ar gas into the system's reservoir tank. A thorough discussion of the effects of water radiolysis on corrosion and mitigation methodology has been presented elsewhere [10].

2.3. Proton beam characteristics

The flux of the incident proton beam had a Gaussian distribution of $2\sigma \approx 3.5$ cm. The energy of this particle beam was 800 MeV. The pulsed beam was characterized by a gate length (macropulse), a macropulse repetition rate, and a peak current as noted in the text (Fig. 2). Average proton beam currents were controlled by varying peak current, gate length and repetition rate. Nominally, the average proton beam currents were varied between 0.01 and 0.4 mA.

2.4. Electrochemical measurements

EIS [11–13] was used to measure the polarization resistance of each sample as a function of average beam current and irradiation time. EIS is ideally suited for this system given the potentially large solution resistance of deionized water. To maximize the signal-to-noise ratio, measurements were conducted with a 30 mV peak-to-peak sinusoidal voltage perturbation [2] over the frequency range of 0.005–1000 Hz. No applied dc potential was employed; that is, all measurements were conducted at the open circuit potential (OCP). To eliminate the effects of ground loops, a floating ground EIS system was used. In these measurements, the traditional three electrode set-up was employed. Here the 304 SS water system acted as the counter electrode. Because a traditional reference electrode was not capable of withstanding the proton/neutron flux at the manifold, one of the in-beam corrosion probes was used as a reference.

All electrochemical measurements were conducted while the proton beam was on.

[2] Although a 30 mV perturbation is somewhat higher than that typically used in EIS measurements, for metals undergoing passive dissolution the effect of an applied anodic voltage is to thicken the passive film. However this increase is small. Therefore, no appreciable effect of the 30 mV signal sample is anticipated.

3. Results and discussion

3.1. Experimental data

Typical EIS data for SS 316L during proton irradiation are shown in Fig. 3. To obtain polarization resistance (R_{pol}) from the EIS data and ultimately corrosion rate, complex non-linear least squares (CNLS) fitting of the data was employed. A simplified Randles equivalent circuit (EC) (Fig. 4) produced a satisfactory fit to the data as seen in Fig. 3. In this EC, R_{pol} represents the polarization resistance and is inversely proportional to corrosion rate, C_{dl} represents the double-layer capacitance, and R_{sol} represents the geometric solution resistance. It has been shown that the phase data are more accurately fit by replacing C_{dl} with a constant phase element (CPE) [5]. As our proton beam modeling required the use of a capacitance, we have chosen to fit our data to C_{dl} directly as opposed to fitting to a CPE and converting back to capacitance. It should be noted that the CPE and C_{dl} models produced similar values for R_{pol}. Uniform corrosion rates in μm/yr of irradiation (CR) were calculated from R_{pol} and the well known expression

$$\mathrm{CR}_{\mu m/yr} = \frac{3.27 \times 10^5 (0.026/R_{pol})(\mathrm{EW})}{\rho}, \quad (1)$$

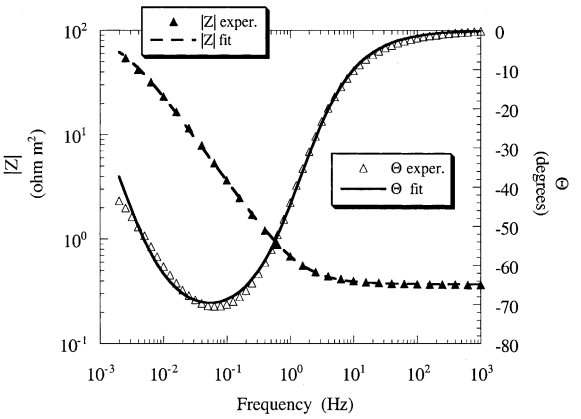

Fig. 3. Bode magnitude and phase plots from the SS 316L sample in tube 36 during proton irradiation at an average proton beam current of 36 μA. The area normalization assumes uniform dissolution across the sample surface.

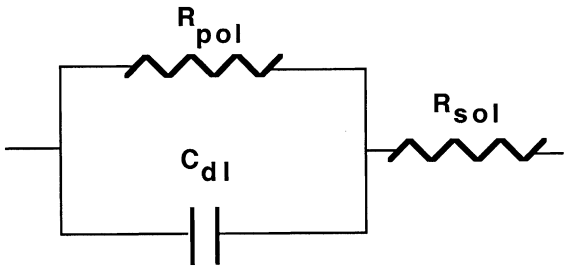

Fig. 4. Equivalent circuit model used in CNLS fitting of the EIS data where: R_{pol} represents the polarization resistance and is inversely proportional to corrosion rate, C_{dl} represents the double-layer capacitance, and R_{sol} represents the geometric solution resistance.

where R_{pol} is the *uniform* polarization resistance (normalized for total area) in $\Omega\,m^2$, EW is equivalent weight and is dimensionless, and ρ is density in kg/m^3. The proportionality constant 3.27×10^5 has units of (μm kg)/(mA m yr). For SS 316L EW is equal to 25.5 and ρ equal to 8.03×10^3 kg/m^3. For alloy 718 EW is equal to 25.7 and ρ is equal to 8.19×10^3 kg/m^3. As seen in Fig. 5, for alloy 718 and SS 316L corrosion rate at any given tube (location) increased with average beam current as observed in previous studies [5]. The relevant duty cycle information for these data can be found in Table 1. In addition to average beam current, location relative to the beam center-line also appears to influence corrosion rate. However, radial distance from the beam does not appear to be the controlling factor as the corrosion rates measured for SS 316L in tube 38 were consistently higher than those measured for SS 316L in tube 35 while both are ≈2.8 cm from the proton beam center (i.e. the center of tube 36). The relationship between sample location and corrosion rate can be seen more clearly in Fig. 6(a) and (b) which are three-dimensional plots of corrosion rate as a function of sample location for SS 316L (at proton beam currents of 0.036 and 0.34 mA). The graphs were created by first plotting the measured corrosion rate for a tube at its distance relative to the beam center. An interpolated mesh between these points was then generated. Thus, when examining these plots the only 'physical data' are that at the positions indicated by tube numbers. The interpolated mesh is an aid that allows the reader to follow trends from one location to another and has no physical significance. As seen in Fig. 6(a) and (b), the highest corrosion rates were observed in tube 36 followed by tubes 38, 35 and 40 in order of decreasing corrosion rate. This trend was observed for all beam currents. It has been proposed that this variation in corrosion rate with sample location is a result of neutron and/or photon flux (Table 2) [5]. For example, although the proton flux is greater at tube 35 as compared to tube 38, both the neutron and photon fluxes are greater at tube 38 consistent with the higher

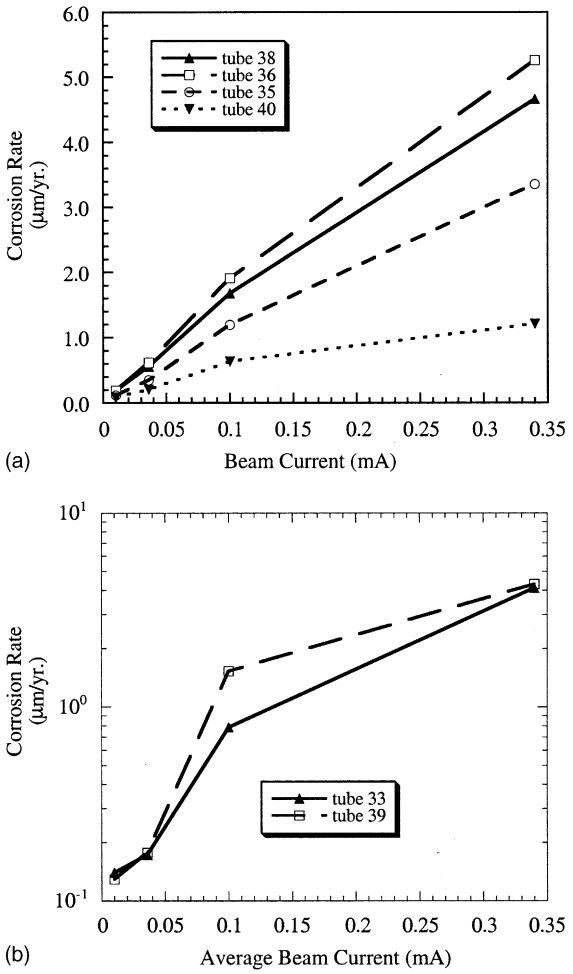

Fig. 5. (a) Corrosion rate (per year of irradiation) as a function of average beam current for the SS 316L probes. Assumes uniform current distribution. (b) Corrosion rate (per year of irradiation) as a function of average beam current for the alloy 718 probes. Assumes uniform current distribution.

Table 1
Proton beam parameters for corrosion data reported in Fig. 5

Average current (mA)	Peak current (mA)	Repetition rate (Hz)	Gate length (μs)	Duty cycle (cycles)
0.010	16	3	200	0.0006
0.036	16	10	200	0.002
0.10	16	10	625	0.00625
0.34	16	36	625	0.0225

corrosion rates reported for tube 38. Similar trends between neutron/photon flux and corrosion rate were observed for all beam currents.

A second set of measurements, termed 'duty cycle experiments,' explored a range of beam delivery pa-

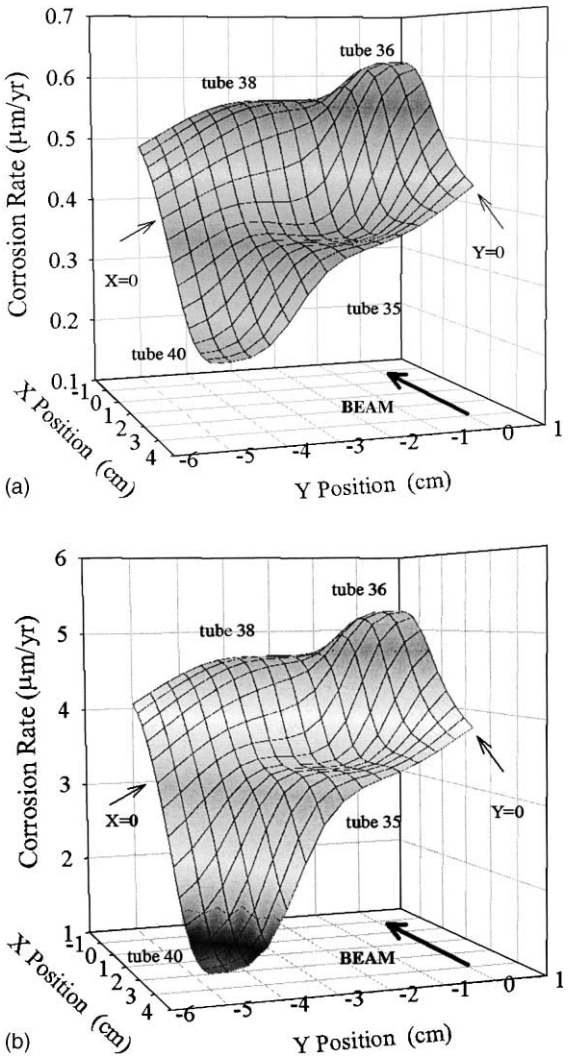

Fig. 6. Three-dimensional plots of corrosion rate (per year of irradiation) as a function of sample location for SS 316L (a) at a proton current of 0.036 mA and (b) at a proton current of 0.34 mA. The graphs were created by first plotting the measured corrosion rate for a tube at its XY position relative to the beam center (0,0 the center of tube 36, see Fig. 1). An interpolated mesh between these points was then generated. Thus, when examining these plots the only 'physical data' is that at the positions indicated by tube numbers.

rameters (peak proton beam current, proton pulse width and repetition rate). [3] The experiment employed two peak currents, the maximum available (16 mA) and another ten times smaller (1.6 mA). The average current

[3] There is an underlying micropulse structure comprised of sub-nanosecond pulses at 5 ns spacing (micropulse spacing in Fig. 2), but this time structure was not considered in this analysis.

Table 2
Results from radiation transport calculations for tubes containing SS 316L samples (calculated at 0.34 mA)[a]

Tube #	Proton flux (p/m^2 s mA)	Neutron flux (n/m^2 p)	Photon flux (γ/m^2 p)
35	72.7	38.0	35.2
36	127	52.7	46.2
38	70.9	43.8	37.3
40	6.0	13.5	13.2

[a] Flux was averaged over the tube length and summed for all particle energies (from Ref. [5]).

was held constant in these experiments by increasing the repetition rate for the 1.6 mA run by a factor of 10. Corresponding R_{pol} data for alloy 718 are summarized in Table 3 for tube 33 (collected with EIS and analyzed with CNLS as discussed above). It was anticipated that R_{pol} would be inversely proportional to peak current. However, the average R_{pol} for the 1.6 mA peak case was always lower than the 16 mA case; conversely, the corrosion rate was always higher for the 1.6 mA case. Similar trends were observed for SS 316L in tube 36.

3.2. Modeling the influence of beam duty cycle

The observation that, at constant average beam current R_{pol} apparently decreases with decreasing peak current may be rationalized in terms of a transient model where the measured R_{pol} is the time-average response of the system. To expand on this, consider the conceptual model in Fig. 7. Prior to the arrival of a pulse of protons, the interface may be characterized by a polarization resistance (R_{off}). In this model, for each macropulse of protons there is a corresponding instantaneously decreased polarization resistance at the electrochemical interface designated as R_{on}. At the end of the macropulse the polarization resistance returns (instantaneously) to the original level (R_{off}). We will address the implication of a time lag in the polarization resistance in Section 3.3 of this paper (that is, a non-instantaneous response of the interface). For small interfacial capacitances (i.e. where the current through C_{dl} can be neglected) the mathematical equivalent to this model is given by the relationship

$$\frac{1}{(\overline{R}_{pol}+R_{sol})}=-\frac{1-c}{R_{off}+R_{sol}}+\frac{c}{R_{on}+R_{sol}}, \qquad (2)$$

where c is the duty cycle (repetition rate×gate length) and $\overline{R}_{pol}$ is the time-averaged polarization resistance measured by the external circuit (here, the polarization resistance measured by EIS). This expression is derived by first summing the time-average charge that flows across R_{off} and R_{on} to obtain the total current through the circuit and then dividing through by the applied

Table 3
Polarization resistance for alloy 718 from tube 33 as a function of average beam current, peak current, gate length, and repetition rate

Peak current (mA)	Avg. current (mA)	Gate (μs)	Repetition rate (Hz)	R_{pol}/std. dev. (kΩ)	R_s/std. dev. (Ω)	C_{dl}/std. dev. (mF)
16	0.010	600	1	24.6/0.36	563/2	1.4/0.01
16	0.010	200	3	24.3/0.37	522/2	1.5/0.01
16	0.033	200	11	18.4/0.24	556/2	1.4/0.01
1.6	0.010	600	10	16.3/0.19	541/2	1.7/0.01
1.6	0.010	200	31	12.1/0.17	520/2	1.9/0.1
1.6	0.035	605	35	11.2/0.14	512/2	2.0/0.02

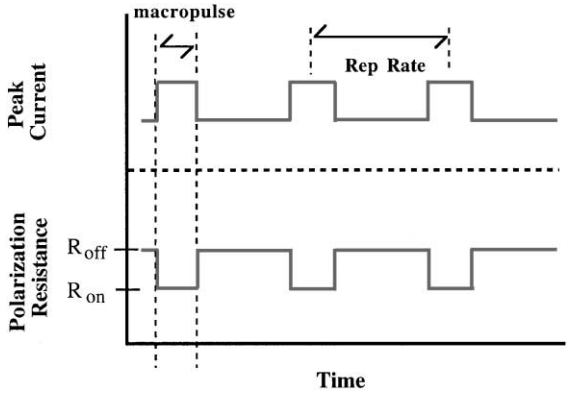

Fig. 7. A diagram for modeling the response of the polarization resistance as a function of proton beam duty cycle. This model assumes that the response of the interface is instantaneous.

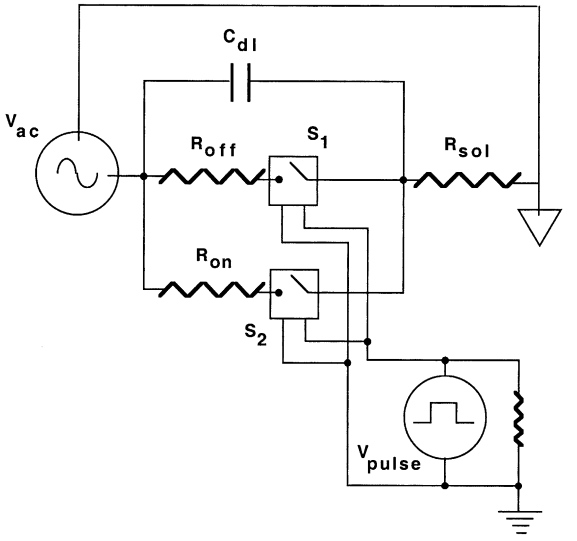

Fig. 8. A schematic diagram of the EC used in SPICE to model the response of the interface to the proton beam (Fig. 7). In this model the square wave generator V_{pulse} was programmed with the same time dependence as the beam duty cycle, such that, a positive voltage (pulse) turned switch S_1 off and S_2 on while a zero voltage turned S_1 on and S_2 off. The electrochemical (measuring) circuit is defined by V_{ac} (30 mV sinusoidal EIS voltage), R_{off}, R_{on} and C_{dl} as noted in the text.

voltage (for EIS this is the voltage of the sinusoidal perturbation). Values for R_{on} and R_{off} can be obtained by measuring $\overline{R}_{pol}$ at a constant peak beam current for various duty cycles and solving Eq. (2) simultaneously for these cases. For our system, the double-layer capacitance of the materials of interest was large (1 mF) and the mathematical simplification in Eq. (2) was insufficient (i.e. the capacitor was associated with a significant fraction of the current) so it was necessary to develop an analytical model which considered C_{dl}).

3.3. SPICE model

The analytical model of the EIS duty cycle data for alloy 718 in Table 3, was developed with the commercially available program SPICE (simulation program with integrated circuit emphasis). SPICE simulates the response of linear and non-linear electrical circuits; it should not be confused with regression analysis such as CNLS used to fit the experimental EIS data. SPICE is capable of real, imaginary, and transient analysis and was, therefore, ideally suited for analyzing the duty cycle data. The EC developed to analyze the data with SPICE is presented in Fig. 8. In this EC, corrosion rate during each macropulse was inversely proportional to R_{on} while corrosion rate between macropulses was inversely proportional to R_{off}. The double-layer capacitance is represented by C_{dl} and the geometric solution resistance between the corroding surface and the reference electrode is represented by R_{sol} as before. In the model, R_{sol} and C_{dl} were taken from the experimental data (Table 3) and held constant while R_{on} and R_{off} are allowed to vary. The pulse generator, V_{pulse}, controls switches S_1 and S_2. By programming the square wave generated by V_{pulse} with the desired beam duty cycle parameters (pulse length and repetition rate) the resistors representing the polarization resistances R_{on} and R_{off} can be connected and disconnected alternately from the circuit simulating the response of the interface to a pulsed proton beam. Impedance data are acquired from the SPICE model in a

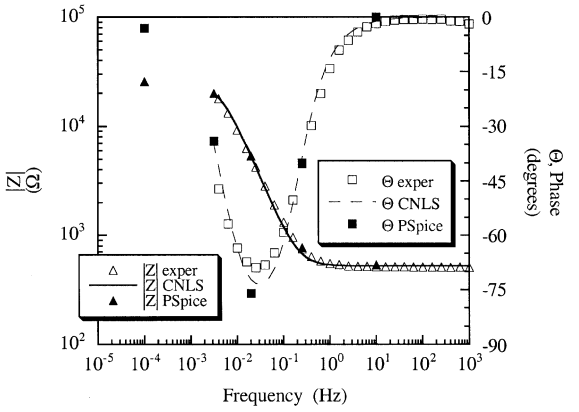

Fig. 9. Experimental Bode magnitude and phase data for alloy 718 (tube 33) during irradiation at 10 μA avg./16 mA peak/3Hz/200 μs. CNLS fit to experimental data and SPICE model results are also shown.

similar manner as it would be experimentally: by applying a 30 mV sinusoidal voltage perturbation across the EC and acquiring the real and imaginary response over the frequency range of 0.1 mH to 1 kHz. The model is said to converge when several conditions are simultaneously met: (1) the low frequency impedance (0.0001 Hz) approaches R_{pol} from the experimental data in Table 3, (2) the Bode magnitude data from SPICE closely agree with the experimental values, and (3) the Bode phase data from SPICE closely agree with the experimental values.

A typical fit of the SPICE model to the experimental data for alloy 718, the CNLS fit of the experimental data, as well as the experimental data are presented in Fig. 9 in the form of Bode magnitude and phase plots. As seen in this figure, good agreement between SPICE, CNLS, and the experimental data were always observed. Table 4 summarizes the results from SPICE modeling of alloy 718 duty cycle data found in Table 3. As might be anticipated the corrosion rate during the beam pulse ($1/R_{on}$) was greater than the rate between pulses ($1/R_{off}$). More importantly, the SPICE model demonstrates that the average corrosion rate ($1/R_{pol}$) is controlled by the duty cycle as well as the average beam current. Thus, for constant average proton beam current, a dc beam would yield a higher corrosion rate than an a pulsed beam at low repetition rate. From these data we also introduce the concept of a corrosion efficiency. It can be seen that the ratio of R_{on} at 1.6 mA peak to R_{on} at 16 mA peak case is less than 10 (5.0) indicating that only a fraction of the energy imparted by each proton on the surface (as power density or in the formation of secondary particles) contributes to the corrosion mechanism. This implies that increasing the peak current to the target may be an effective way of minimizing corrosion damage where higher proton flux is needed. For example, compare the data from the experiment at 1.6 mA peak/10 μA avg./200 μs/31 Hz with the experiment at 16 mA peak/10 μA avg./200 μs/3 Hz (rows 5 and 2 in Tables 3 and 4). Although the model corrosion rate during the beam pulse (R_{on}) is greatest for the 16 mA case, the measured corrosion rate (R_{pol}) is greater for the 1.6 mA case presumably owing to the higher repetition rate. Therefore, a higher peak/lower duty cycle beam produces an equivalent flux at the target with a lower average corrosion rate.

Finally, it is noted that the low values of R_{on} in Table 4 are well within the capability of the impedance equipment used to collect data indicating that the experimental data is not limited by the solution resistance in this case. That is, it appears that time-averaged measurements such as EIS, Tafel extrapolation, and linear polarization resistance can be used to accurately measure corrosion rate during pulsed proton irradiation providing the response is not limited by a critical combination of high R_{sol} and low R_{on}. In that case, the voltage drop across R_{on} would be too low to sense the response of the surface during the beam pulse and the derived corrosion rate would be grossly underestimated. In this regard, an additional consideration is the influence of C_{dl} and the beam gate length which is addressed in Section 3.4.

3.4. Numerical model

To supplement the ac SPICE data, a dc numerical method was used to model the response of the interface to a single transient. The EC used in these simulations is

Table 4
Summary of SPICE results from modeling of the alloy 718 data presented in Table 3

Peak current (mA)	Avg. current (mA)	Gate (μs)	Repetition rate (Hz)	R_{off} (kΩ)	R_{on} (Ω)	R_{pol} @ 0.1 mHz (kΩ)
16	0.010	600	1	37	43	23
16	0.010	200	3	36	40	25
16	0.033	200	11	38	50	15
1.6	0.010	600	10	36	220	16
1.6	0.010	200	31	32	200	13
1.6	0.035	605	35	39	240	12

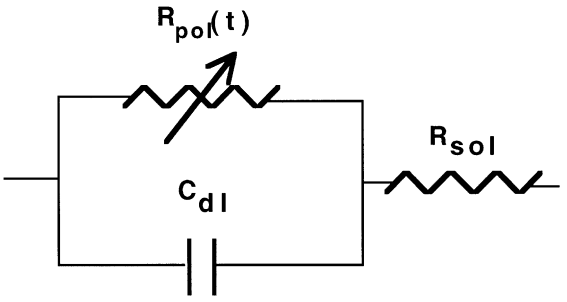

Fig. 10. Equivalent circuit used in the dc numeric modeling method. The variable resistance $R_{pol}(t)$ represents the time dependence of the response of the interface to the pulsed proton beam.

shown in Fig. 10. In this EC, the variable resistance $R_{pol}(t)$ represents the time dependent response of the interface to a beam pulse. As in the SPICE model, the solution resistance and double-layer capacitance were fixed at their experimentally determined values (Table 3). The goal of this model was to determine what type of time dependency (liner, quadratic, power function ...) for $R_{pol}(t)$ best fit the experimental data. A representation of what the response of the interface to the beam might look like is shown in Fig. 11. After several iterations using various expressions for the time dependency for $R_{pol}(t)$, it was determined that two relationships best fit the experimental data. During a beam pulse the polarization resistance was best fit by a linear time dependence [4]

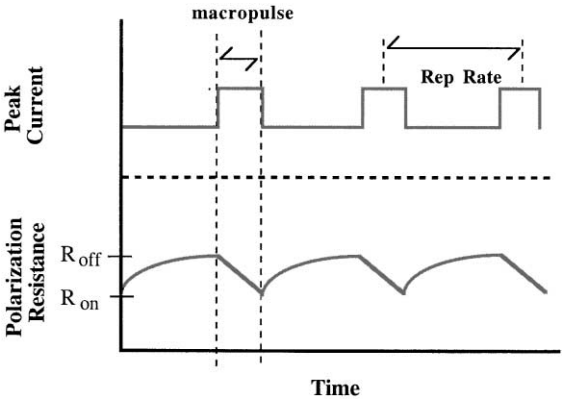

Fig. 11. A diagram for modeling the time dependent response of the polarization resistance as a function of proton beam duty cycle in the dc numerical method. This model assumes that the response of the interface during a beam pulse is linear while the response between pulses is exponential.

[4] The dependence is linear in corrosion rate $1/R_{pol}(t)$.

$$R_{pol}(t) = \frac{R_{on} t_{pl}}{t}, \tag{3}$$

where t is elapsed time in s, and t_{pl} is the pulse length in s, while between pulses the polarization resistance was best fit by an exponential relaxation back to R_{off}:

$$R_{pol}(t) = R_{off} - (R_{off} - R_{on}) \exp\{-\lambda(t - t_{pl})\}, \tag{4}$$

where λ is a decay constant. Although the physical significance of the linear time dependence in Eq. (3) and λ in Eq. (4) is unknown, it might be expected that electrochemical reactions at the interface have a kinetic (time) response. A time dependent response for irradiated interfaces has been reported elsewhere [3].

In the numerical analysis an initial starting value for the capacitor voltage (V_c) was chosen (that is, the voltage division between R_{sol} and R_{off}). The input to the circuit simulation was the time dependent polarization resistance $R_{pol}(t)$. At each step in time through the calculation, a new R_{pol} alters the currents in the circuit:

$$I_{R_{pol}} = \frac{V_c}{R_{pol}(t)}, \tag{5}$$

$$I_{C_{dl}} = \frac{(0.030 - V_c)}{R_{sol}} - \frac{V_c}{R_{pol}(t)}, \tag{6}$$

where 0.03 V is the applied potential in our measuring circuit (i.e. near dc in EIS). The steady state V_c is initially unknown to the calculation and is determined by the condition that V_c at the end of the beam pulse period is the same as V_c at the beginning of the beam pulse. The total current in external circuit was determined by summing Eqs. (5) and (6).

With the numerical model, several corrosion observations can be fit simultaneously, for example, the data from each set of peak currents in the alloy 718 duty cycle series (Table 3). In these analyses, a boundary condition was imposed which mandated that R_{off} be the same for the both the 1.6 and 16 mA experiments. This condition is consistent with the observation in previous studies that the polarization resistance increases after turning the beam off [3]. With this boundary condition, the 16 mA data were best fit by values of 88 Ω for R_{on} at $t_{pl} = 600$ μs ($R_{on} t_{pl} = 0.0053\ \Omega\,s^{-1}$). For the 1.6 mA case, a satisfactory fit was found for R_{on} (at 600 μs) equal to 880 Ω Table 5). In both the 16 and 1.6 mA fits, λ was held constant at an optimized value of 85.0 s^{-1}. Fig. 12 illustrates the behavior of $R_{pol}(t)$ from the numeric modeling and the resulting current flowing through the sample surface for the 600 μs beam pulse, 1.6 mA peak proton beam current, and a repetition rate of 10 Hz. case. Of the total charge transferred across the surface 8% is delivered during the beam pulse and the remaining 92% between pulses. In comparison, in the square-step

Table 5
Summary of the dc numeric results from modeling of the alloy 718 data presented in Table 3

Peak current (mA)	Avg. current (mA)	Gate (μs)	Repetition rate (Hz)	R_{off}; fixed (kΩ)	R_{on} @ 600 μs (Ω)	R_{pol} (kΩ)
16	0.010	600	1	28.2	88	24.2
16	0.010	200	3	28.2	88	23.6
16	0.033	200	11	28.2	88	16.4
1.6	0.010	600	10	28.2	880	18.7
1.6	0.010	200	31	28.2	880	14.8
1.6	0.035	605	35	28.2	880	10.3

SPICE model for the same duty cycle case, of the total charge transferred across the surface, 50% is delivered during the beam pulse and the remaining 50% between pulses. This difference between the allocation of charge is a result of the necessity in the SPICE model that R_{on} and R_{off} remain fixed (i.e. the interface is modeled as having a stepped response). While SPICE has the advantage of modeling the ac response of the system which provides real and imaginary data for comparison with the actual experiment, the ability to vary the response of the interface with time for given R_{on} and R_{off} in our dc numeric model (and, therefore, preferentially distribute the charge) results in more accurate fits of the numerical method to the experimental data for the 16 mA peak current case.

The pulsed beam models constructed in SPICE and the dc numerical method predict that large charge transfer currents flow during the beam pulse and then diminish before the next pulse. During the course of a corrosion measurement, the double-layer capacitance was large enough in these materials (on the order of 1–2 mF) such that the large pulsed currents will be smoothed out by the RC time constants. Specifically, the large

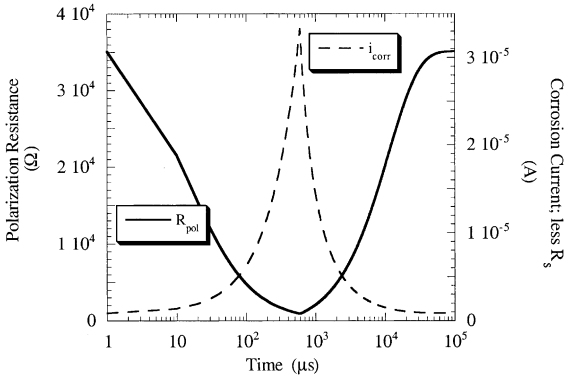

Fig. 12. Numerical model – polarization resistance $R_{pol}(t)$ as a function of time. Current flowing through the sample surface. 30 mV dc is applied by the external circuit. The case is 600 μs beam pulse, 1.6 mA peak proton beam current, and a repetition rate of 10 Hz.

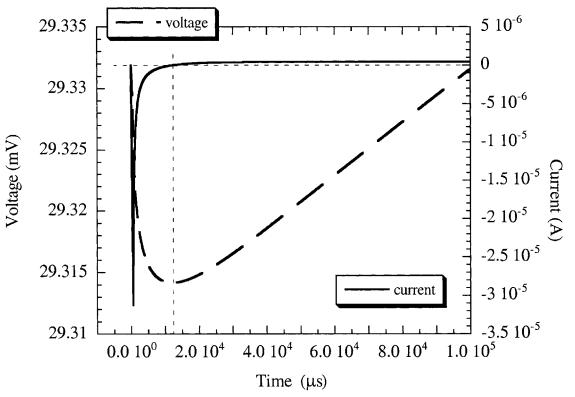

Fig. 13. Voltage and current response of C_{dl} to a beam pulse (from dc numeric model). Negative current represents current that flows from the capacitor across $R_{pol}(t)$ and is consumed on the opposite terminal. Positive current after 1.2×10^4 s represents current through the measuring circuit (that is, recharging of the capacitor).

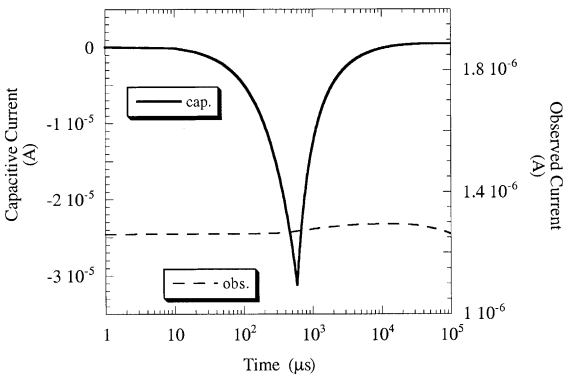

Fig. 14. Numerical model – influence of the capacitance (2 mF) for the same duty cycle parameters as in Fig. 11. The capacitor current approximates the charge transfer current while the current in the external circuit is relatively steady due to the recharge of the capacitor through the solution resistance. The capacitor voltage stays near 29.3 mV dc the entire time.

charge transfer current discharges the double-layer capacitance during the transient, and the measuring

device records a relatively smooth average current as the capacitance recharges between proton pulses. To illustrate this, the response of the double-layer capacitor is presented in Fig. 13. In this figure at time equal to zero, a beam pulse arrives at the interface. The decrease in $R_{pol}(t)$ causes the capacitive voltage to drop resulting in a sharp increase in the capacitive current (that is, C_{dl} is discharging across a smaller R_{pol}). At the end of the beam pulse (time equal to 600 μs) $R_{pol}(t)$ begins to increase and the current from the discharging C_{dl} begins to decrease. The capacitive voltage does not reach its minimum of 29.314 mV until $\approx 1.2 \times 10^4$ s. Up until this time, little current flows through the measuring circuit as only 0.7 mV is being dropped across R_{sol}. After 1.2×10^4 s, the increase in R_{pol} causes the capacitive voltage to increase resulting current flow in the external circuit (Fig. 14 [5]).

4. Conclusions

We have described a model for analyzing corrosion data collected during pulsed proton beam irradiation. In this model two independent polarization resistances were used to represent the response of the interface; R_{on} representing the response during a pulse of protons and R_{off} the response between pulses. The model was verified using two independent methods; SPICE, an analog circuit simulation program for ac analysis and a dc numerical method. With this model we have demonstrated that time-averaged measurements such as EIS, Tafel extrapolation, and linear polarization resistance can be used to accurately measure corrosion rate during pulsed proton irradiation. In addition, the model explains an apparent anomaly in corrosion rate data. During irradiation at a peak proton beam current of 1.6 mA the corrosion rates were (in general) higher than those measured during irradiation at 16 mA at the same average proton beam current. The model shows that, although $1/R_{on}$ directly correlates with peak current (i.e. $1/R_{on}(16\text{ mA}) > 1/R_{on}(1.6\text{ mA})$), the time-averaged corrosion rate measured by electrochemical techniques is controlled by duty cycle (pulse length and repetition rate) as the relationship between corrosion efficiency and proton flux was not 1 to 1 (i.e. the ratio of $R_{on}(16\text{ mA})/R_{on}(1.6\text{ mA})$ was less than 10). Therefore, for an equivalent average proton beam current, lower peak currents will necessarily be associated with larger duty cycles and greater corrosion rates. From these results we have concluded that the most efficient way of maximizing proton flux and simultaneously minimizing corrosion rate is by using a high peak current.

[5] The data in Fig. 14 are presented on a log(time) scale so that detail could be seen. As a result, the area under the capacitive current curve before and after the capacitive voltage reaches its minimum does not appear to be equal nor does capacitive current curve after the voltage minimum appear to equal the small increase in the observed current. However, these currents are in fact equal as can be seen in Fig. 13.

Acknowledgements

Work on this project was performed by the University of California under the auspices of the United States Department of Energy contract W7405-ENG36. The authors would like to thank Laurie Waters and the support of the APT Project Office, Darryl Butt (UF), Frank Gac, Stuart Maloy, Mike James and Luke Daemen for helpful discussions; Gordon Willcutt for thermahydraulic design; Phil Ferguson (ORNL) for radiation transport calculations; Richard Werbeck, Michael Baumgartner, Bob Brown, and the rest of the LANSCE-7 group for their engineering expertise putting the experiment together; R.G. Stone and R.E. Loehman (Sandia National Lab) for manufacturing some of the corrosion probes.

References

[1] R.S. Lillard, D.P. Butt, J. Mater. 50 (1998) 56.
[2] R.S. Lillard, D.P. Butt, Mater. Characteriz. 43 (1999) 135.
[3] R.S. Lillard, G.J. Willcutt, D.L. Pile, D.P. Butt, J. Nucl. Mater. 277 (2000) 250.
[4] W. Sommer, S. Maloy, M. Zaslawsky, in: 2nd International Workshop on Spallation Materials Technology, Ancona, Italy, 1997.
[5] R.S. Lillard et al., in: S.T. Rosinski, M.L. Grossbeck, T.R. Allen, A.S. Kumar (Eds.), Effects of Radiation on Materials: 20th International Symposium, ASTM STP 1405, ASTM, West Conshohocken, PA, 2001, p. 631.
[6] M.E. Indig, J.E. Weber, Corrosion/83, NACE, Houston, TX, 1983, paper no. 124.
[7] M. Fox, Corrosion/83, NACE, Houston, TX, 1983, paper no. 123.
[8] M.J. Fox, A Review of Boiling Water Reactor Chemistry: Science, Technology, and Performance, Argonne National Laboratory for the US Nuclear Regulatory Commission NUREG/CR-5115 ANL-88-42, 1989.
[9] C.C. Lin, R.L. Cowan, R.S. Pathania, Corrosion/93, NACE, Houston, TX, 1993, paper no. 619.
[10] R.S. Lillard, D.L. Pile, D.P. Butt, J. Nucl. Mater. 278 (2000) 277.
[11] D.D. MacDonald, in: F. Mansfeld, U. Bertocci (Eds.), Electrochemical Corrosion Testing, ASTM STP 727, ASTM, Philadelphia, PA, 1981, p. 110.
[12] J.R. MacDonald, Impedance Spectroscopy, Wiley, New York, 1987.
[13] M. Sluyters-Renbach, J.H. Sluyters, Electroanal. Chem. 4 (1) (1970) 1.